Top Catal (2016) 59:196–206
DOI 10.1007/s11244-015-0428-3

ORIGINAL PAPER

Conversion of Biomass-Derived 2-Hexanol to Liquid Transportation Fuels: Study of the Reaction Mechanism on Cu–Mg–Al Mixed Oxides

P. J. Luggren[1] · C. R. Apesteguía[1] · J. I. Di Cosimo[1]

Published online: 30 July 2015

Abstract The reaction mechanism of 2-hexanol conversion to high molecular weight compounds to be used as liquid transportation fuels was studied on MgO, Cu/SiO_2 and a bifunctional Cu–Mg–Al mixed oxide with 8 wt% Cu (catalyst 8.0CuMgAl). Catalysts were characterized by several physical and spectroscopic techniques. The evolution of 2-hexanol conversion and yields in inert (N_2) and reducing (H_2) reaction atmospheres at different contact times (W/F^0) was investigated, which allowed distinguishing between primary and secondary products. In H_2, at $W/F^0 = 500$ g h/mol, the bifunctional 8.0CuMgAl catalyst yielded more than 90 % of branched C9–C24 oxygenates and hydrocarbons that were obtained via sequential steps comprising dehydrogenation, C–C coupling, dehydration and hydrogenation reactions. The metal-base bifunctional nature of this reaction network on 8.0CuMgAl was elucidated: nano-sized Cu^0 particles promote dehydrogenation and hydrogenation steps whereas Mg–O pairs participate mainly in C–C coupling reactions. The product distribution depended on the reaction atmosphere. In H_2, the reaction pathways leading to formation of even carbon atom number products (C12, C18 and C24) were favored and hydrocarbons were the main products at high conversion levels. In N_2, significant amounts of odd carbon atom number products (C9, C15 and C21) were formed with a higher contribution of oxygenates to the product pool.

✉ J. I. Di Cosimo
dicosimo@fiq.unl.edu.ar

[1] Catalysis Science and Engineering Research Group (GICIC), INCAPE, UNL-CONICET, Santiago del Estero 2654, 3000 Santa Fe, Argentina

Keywords 2-Hexanol · Aldol condensation · Dehydrogenation · Hydrogenation · Copper · Mixed oxides

1 Introduction

Biorefineries represent a novel paradigm for development of new environmentally friendly processes. Energy, fuels and chemicals can be produced in a sustainable manner by transforming bio-based resources using intensified processes [1, 2]. For example, lignocellulose, an abundant and inexpensive feedstock, can be transformed by different thermal, chemical and biological treatments into chemical species that are easier to process, such as sugars. Then, conversion of sugars in the biorefinery may result in the production of liquid transportation fuels [3, 4] which consist of nonoxygenated hydrocarbons in the range of C5–C12 for gasoline, C9–C16 for jet fuel and C12–C20 for diesel [5].

Second generation liquid biofuels derived from carbohydrates do not compete with food supply and their combustion has a zero CO_2 balance. However, sugars are C5–C6 compounds with high oxygen content (O:C = 1:1) and therefore, their suitable conversion in the biorefinery requires removal of almost all the oxygen atoms by hydrogenolysis, dehydration or hydrogenation reactions [4, 6]. In addition to deoxygenation, other processes must take place such as isomerization to form branched hydrocarbons for gasoline, and/or by C–C coupling reactions to increase the molecular weight for diesel and jet fuels [6].

These ideas were applied by Kunkes et al. [6] who postulated a strategy to convert carbohydrates in liquid fuels by oxygen removal at 500 K on a Pt–Re/C catalyst. Products are a well-defined mixture of hydrophobic species with 4–6 carbon atoms and 1–2 oxygen atoms. This first step removes more than 80 % of the carbohydrate oxygen.

The hydrophobic mixture contains the so called "platform molecules" such as ketones, carboxylic acids, secondary alcohols and heterocyclic compounds (furans) which can be further transformed into C9–C18+ alkanes for liquid transportation fuel applications. For the upgrading of the C4–C6 organic liquid stream to C6–C12 compounds at 573 K and 5 bars of H_2, Kunkes et al. [6] postulated the use of a Cu–Mg–Al mixed oxide previously used in our group for C–C bond forming applications [7]. On that catalyst, they showed that 45 % of the carbon in the product mixture is associated with the C8–C12 product fraction and contains one or none oxygen atoms.

We have shown in previous works that Cu–Mg–Al mixed oxide catalysts can be successfully used in other applications requiring a combination of metallic and acid–base sites: (i) Conversion of alcohols, such as 2-propanol, proceeds at high rates on these catalysts by a sequence of steps that comprises dehydrogenation/aldol condensation/dehydration/hydrogenation reactions [7, 8]. (ii) The gas-phase hydrogen-free reduction of α,β-unsaturated ketones selectively forms saturated ketones on these catalysts [9]. (iii) The upgrading of polyols (1,3-butanediol) on these materials gives valuable oxygenates by either dehydrogenation or dehydration reactions, depending on the copper loading [10]. Recently, other researchers have shown that similar Cu–Mg–Al mixed oxides promote C–C coupling [11, 12], aqueous phase hydrogenation [13] and several oxidation [14–16] reactions, among many other applications.

In this work, 2-hexanol was chosen as a model platform molecule of the sugar transformation. We report the gas-phase synthesis of liquid transportation fuels from 2-hexanol on a Cu–Mg–Al mixed oxide with 8 wt% Cu (catalyst 8.0CuMgAl), MgO and a Cu/SiO_2 catalyst. The bifunctional metal-base 8.0CuMgAl catalyst that combines a well dispersed metallic function provided by copper with moderate acid–base properties gave the best results.

The bifunctional nature of the catalytic process leading to formation of C9–C24 oxygenates and hydrocarbons was investigated as well as the role played by each active site in the reaction sequence that involves tandem dehydrogenation/C–C coupling/dehydration/hydrogenation steps. The reaction pathways operating under different reaction conditions were elucidated. The effect of co-feeding H_2 on the catalyst activity, product distribution and oxygen content of the product mixture was also discussed.

2 Experimental

2.1 Catalyst Synthesis and Characterization

Sample 8.0CuMgAl (8 wt% Cu) was prepared by coprecipitation at a constant pH of 10, as detailed elsewhere [7]. Briefly, the ternary Cu–Mg–Al catalyst precursor (Mg/Al = 1.5 and Mg/Cu = 10, molar ratios) of hydrotalcite structure was filtered, washed and dried at 363 K; then it was placed in a reactor and decomposed overnight in flowing air (25 cm^3/min) at 773 K in order to obtain the corresponding mixed oxide. A ramp rate of 5 K/min was used. High-surface area magnesium oxide was prepared by hydration with distilled water of low-surface area commercial MgO (Carlo Erba 99 %; 27 m^2/g) and further decomposition of the resulting $Mg(OH)_2$ in a N_2 flow for 18 h at 773 K [17]. The silica-supported 8.5CuSi catalyst with 8.5 wt% Cu was prepared by ion exchange through the so called "chemisorption-hydrolysis" technique, using a Evonik Aerosil 380 silica support, as described in [18]. Samples were sieved to retain particles in the 0.177–0.500 mm range and this fraction was used in the characterization experiments.

BET surface areas (*SA*) were measured by N_2 physisorption at its boiling point using an Autosorb Quantachrome 1-C sorptometer. The sample structural properties were determined by X-ray diffraction (XRD) technique using a Shimadzu XD-D1 instrument. The Cu chemical content of the catalyst was analyzed by Atomic Absorption Spectrometry (AAS).

Catalyst base site number (n_b) was measured by temperature-programmed desorption (TPD) of CO_2 preadsorbed at room temperature. After exposing 50 mg of the sample to a flowing mixture of 3 % of CO_2 in N_2, weakly adsorbed CO_2 was removed by flushing with N_2. Finally, the temperature was increased to 773 K at a ramp rate of 10 K/min. The desorbed CO_2 was converted into CH_4 on a Ni/Kieselghur catalyst at 673 K and then analyzed using a flame ionization detector (FID) [7]. The acid site number, (n_a) was determined by TPD of NH_3 preadsorbed at room temperature. After pretreating 50 mg of the sample in He at 773 K for 1 h, it was exposed at room temperature to a flow of 1.01 % NH_3/He until surface saturation. Weakly adsorbed NH_3 was removed by flowing 60 cm^3/min of He; the temperature was then increased to 773 K at 10 K/min. The NH_3 concentration in the effluent was analyzed by mass spectrometry (MS).

The dispersion of the metallic copper particles (*D*), defined as the ratio of the number of surface metallic copper atoms (Cu^S) to the total copper atoms in the catalyst measured by ASS (Cu^T_{AAS}), was calculated by combining temperature programmed reduction (TPR) and N_2O decomposition. Details are described in [10, 18]. In the TPR experiments, a reducing mixture of 5 % H_2/Ar at a flow rate of 50 cm^3/min was used; the reactor was loaded with a molar amount of copper (150 μmol) so that to meet the criteria of Monti et al. [19] and Malet et al. [20]. A heating rate of 10 K/min from 298 to 623 K was used. A mass spectrometer (MS) in a Baltzers Omnistar unit monitored the hydrogen consumption. Quantitative H_2-uptakes were

calculated by integration of the experimental TPR curves and using a previous calibration curve with CuO powder (Cicarelli, PA). The Cu^S value was determined from the TPR experiment carried out after re-oxidation at 363 K of the surface copper metal atoms to Cu_2O using pulses of N_2O (5×10^{-3} cm^3) and a stoichiometry of $Cu^S/N_2O = 2$. The number of exposed Cu^0 species was calculated as n_{Cu} (μmol/g cat) = $157 \times D \times Z$ (Z = wt% Cu) and the average copper particle size as L (nm) = $1.04/D$.

2.2 Catalytic Testing

Vapor-phase conversion of 2-hexanol (C6OL) was carried out at 573 K and 101.3 kPa in a fixed-bed reactor at contact times (W/F^0_{C6OL}) of 11–500 gcat h mol of $C6OL^{-1}$. Catalysts were loaded as 0.177–0.500 mm particles in which intra-particle diffusional limitations were verified to be negligible. Samples were pretreated in a flow of N_2 at 773 K for 1 h before the catalytic tests, then they were reduced in situ in flowing H_2 (35 cm^3/min) at 573 K for 1 h. The reactant, C6OL (Aldrich ≥98.0 %), was introduced via a syringe pump and vaporized into flowing N_2 or H_2 to give a pressure ($\bar{P}_{C6OL}$) of 4.1 kPa. Reaction products were analyzed by on-line gas chromatography using an Shimadzu GC-2014 chromatograph equipped with flame ionization detector and a (5 % phenyl)-methylpolysiloxane HP-5 Agilent capillary column. Data were collected every 0.5 h for 5 h. Unknown species were identified using a Varian Saturn 2000 GC/MS with a NIST library of spectra. Products are denoted as C6K (2-hexanone), CnO (oxygenates), CnH (hydrocarbons), CnK (saturated ketones), CnUK (unsaturated ketones) and CnOL (alcohols), where n is the carbon atom number in the molecule. Due to a slight catalyst deactivation process, the catalytic results were calculated by extrapolation of the reactant and product concentration curves to zero time on stream. Then, X_{C6O}, S and Y represent conversion, selectivity and yield at t = 0, respectively. The equilibrated nature of C6OL-C6K interconversions [21] at the present reaction conditions, allows us to consider these two molecules hereinafter as the reactant pool. Thus, conversion was defined for the reactant pool (C6O = C6OL + C6K) as:

$$X_{C6O} = \left(1 - \frac{F_{C6OL} + F_{C6K}}{F^0_{C6OL}}\right)$$

where F_{C6OL} and F_{C6K} are the molar flow rate of C6OL and C6K, respectively, at the reactor exit; F^0_{C6OL} is the molar flow rate of C6OL in the reactor feed.

Product selectivity was calculated on a carbon atom basis, as:

$$S_i = \frac{F_i N_i}{\sum_i F_i N_i}$$

where N is the carbon atom number of product "i". Carbon balances closed to within 4–8 %.

Pool turnover rates (TOR) are defined as the moles of C6O converted per mol of Cu^0 surface site and per second.

3 Results and Discussion

3.1 Catalyst Characterization

In the metal-base bifunctional 8.0CuMgAl catalyst, copper was chosen to provide a metallic function whereas Mg^{2+} and Al^{3+} cations were selected because of the known acid–base properties of their corresponding single or mixed oxides. The Cu–Mg–Al elemental combination was shown to be suitable for conversion of alcohols and polyols [7, 9, 22]. In particular, previous results showed that Cu loadings of around 8wt% give rise to mixed oxides with a proper combination of metallic and basic sites to promote chain lengthening reactions at high rates [23].

On the other hand, MgO and 8.5CuSi catalysts were prepared to represent typically, basic and metallic monofunctional catalysts, respectively.

The 8.0CuMgAl sample as well as the reference MgO and 8.5CuSi catalysts were characterized by several techniques. The physicochemical properties of the catalysts prepared in this work are summarized in Table 1. The identification of the crystalline phases present in the oxides was carried out by XRD (diffractograms not shown here). In Cu-containing oxides, no crystalline copper species was detected and they only showed the single quasi-amorphous MgO or SiO_2 phase. Thus, copper species are probably highly dispersed as small CuO crystallites not detectable by XRD. On the other hand, the contraction of the MgO unit cell (a_{MgO}) in the 8.0CuMgAl mixed oxide (4.150 Å) compared with that of pure MgO (4.216 Å) is the result of substitution of smaller Al^{3+} cations ($r_{Al^{3+}} = 0.535$ Å) for Mg^{2+} ($r_{Mg^{2+}} = 0.72$ Å) in the structure, Table 1 [24, 25].

The reducibility of Cu species the copper-containing samples was investigated by TPR, Fig. 1. Quantification of the reduced copper species was carried out considering that the observed H_2 consumption peaks of Fig. 1 correspond to $Cu^{2+} \rightarrow Cu^0$ reduction [26]. The 8.0CuMgAl sample reduced giving a single and broad reduction peak at around 550–600 K with a temperature at peak maximum (T_M) of 571 K. Similarly, sample 8.5CuSi showed also a broad peak with a T_M value of 532 K, a value closer to that of

Table 1 Physicochemical properties of 8.0CuMgAl, MgO and 8.5CuSi catalysts

Catalyst	Surface area, *SA* (m^2/g)	Nominal composition (wt%)			Structural analysis by XRD		Cu species reducibility, dispersion and size				Acid–base properties (μmol/g)	
		Cu	Mg	Al	a_{MgO}[a] (Å)	Phases detected	D[b] (%)	n_{Cu}[c] (μmol/g)	L[d] (nm)	T_M[e] (K)	n_b[f]	n_a[g]
8.0CuMgAl	248	7.8	29.7	21.4	4.150	MgO	12	154	8.5	571	457	124
MgO	189	–	60.3	–	4.216	MgO	–	–	–	–	655	15
8.5CuSi	225	8.0	–	–	–	SiO_2	27	368	3.8	532	–	–

[a] MgO lattice constant

[b] Cu^0 dispersion by N_2O decomposition

[c] Number of exposed Cu^0 species

[d] Cu^0 particle size

[e] Temperature at peak maximum by TPR

[f] Base site number by TPD of CO_2

[g] Acid site number by TPD of NH_3

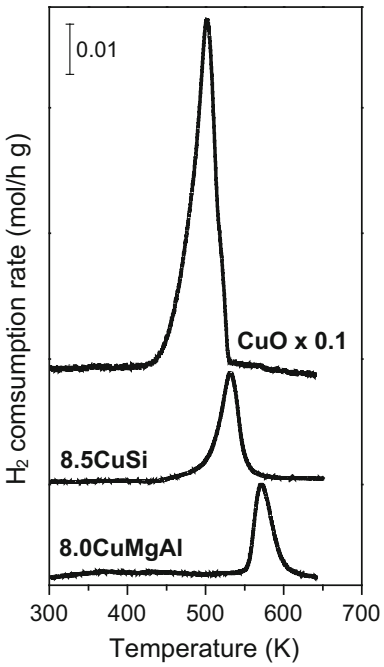

Fig. 1 TPR profiles of 8.0CuMgAl and 8.5CuSi. CuO included as reference

pure reference CuO (502 K) [10]. The differences in reducibility of both samples is assigned to the different preparation procedures and the resulting chemical environments of the copper species. In the sample prepared by coprecipitation, formation of a solid solution in which small amounts of Cu^{2+} replace Mg^{2+} within the MgO structure is favored by the slight difference in ionic size between Cu^{2+} ($r_{Cu^{2+}} = 0.73$ Å) and Mg^{2+}. This probably gives rise to a strong Cu-mixed oxide interaction that explains the higher temperature needed to completely reduce CuO in sample 8.0CuMgAl. The copper dispersion was higher in 8.5CuSi ($D = 27$ %) than in 8.0CuMgAl ($D = 12$ %), thereby confirming that preparation of Cu-supported catalysts by the chemisorption-hydrolysis method leads to the formation of smaller Cu particles [27].

The surface base and acid properties of the 8.0CuMgAl, 8.5CuSi and MgO catalysts were investigated by TPD of CO_2 (Fig. 2) and NH_3 (Fig. 3), respectively. The total number of base sites (n_b, μmol/g) was calculated by integration of the CO_2 TPD curves and results are shown in Table 1; the number of acid sites (n_a, μmol/g) was determined in a similar fashion from the TPD curves of Fig. 3 (Table 1). Similarly to pure MgO, sample 8.0CuMgAl desorbed CO_2 in a wide temperature range of 350–700 K, reflecting the presence of a distribution of surface sites that adsorb CO_2 with different binding energies. However, the presence of acidic Al^{3+} cations in the formulation of 8.0CuMgAl shifts the peak maximum to lower temperatures and decreases the n_b value compared to MgO (Table 1). The Al-containing sample 8.0CuMgAl showed a higher n_a value than MgO. Sample 8.5CuSi does not contain any measurable acid or base sites.

3.2 Bifunctional Catalysis

The synthesis of compounds to be used as liquid transportation fuels (C9–C24 oxygenates and hydrocarbons) by gas-phase conversion of C6OL was studied on catalyst 8.0CuMgAl and reference MgO and 8.5CuSi samples. The reaction products were in the C3–C24 carbon atom range. Formation of these compounds involves several reaction steps as depicted in Scheme 1. The reaction sequence starts

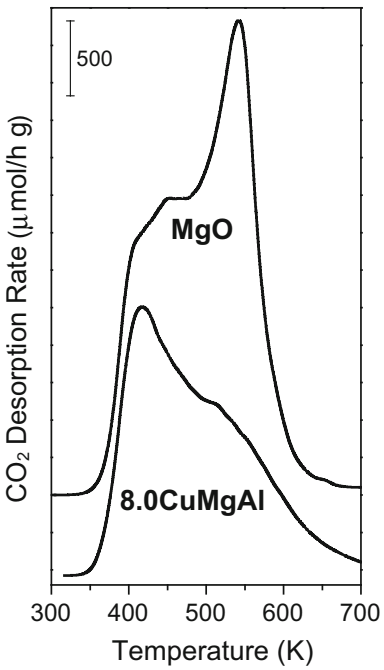

Fig. 2 TPD of CO_2 on 8.0CuMgAl and MgO

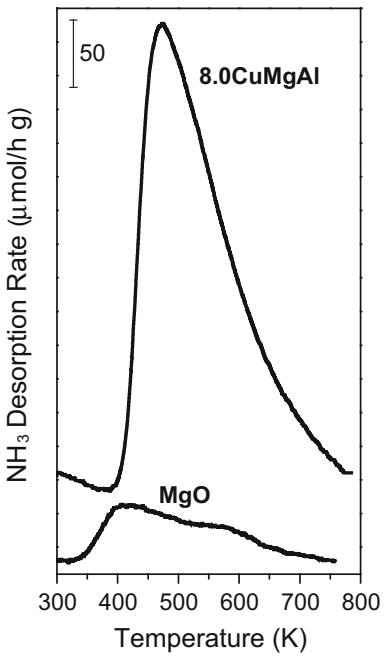

Fig. 3 TPD of NH_3 on 8.0CuMgAl and MgO

by the dehydrogenation of C6OL to C6K (block C6O), but C6OL may also be converted to C6H via a dehydration-hydrogenation reaction pathway (block C6H). Alcohol dehydration and formation of short chain compounds such as C3OL, C3K and C3H (block C3) by C–C bond cleavage are likely to occur on Cu-based catalysts [22], but they are undesirable for the present purposes. Then, the initial C6OL conversion to C6K may be challenging because of the catalyst acidic properties needed to promote the dehydration steps participating in the process. In the same way, Cu was chosen to provide the metallic site because preferentially dehydrogenates alcohols, giving aldehydes or ketones at mild temperatures without significantly breaking the C–C bonds.

After C6K formation, the C9–C24 product synthesis entails a base-catalyzed C–C bond forming aldol condensation reaction as part of a series of consecutive reaction steps that comprises dehydrogenation, C–C coupling, dehydration and hydrogenation reactions, Scheme 1. The selection of the proper basic properties is also difficult because base sites promote not only the aldol condensation steps but also the detrimental base-catalyzed C–C bond cleavage reactions leading to light compounds [22].

The catalytic performance of 8.0CuMgAl and reference MgO and 8.5CuSi catalysts is reported in Table 2. For the reasons explained in section 2.2, we considered the reactant pool as C6O = C6OL + C6K in our calculations. The C6O conversion (r_{C6O}) and turnover (TOR) rates as well as the selectivity to C3 (S_{C3}), C6H (S_{C6H}) and C9–C24 compounds (S_{C9-C24}) at 20 % conversion are shown in Table 2.

Since sample 8.5CuSi does not contain any measurable acid or base sites, it was selected to investigate the participation of the Cu^0 sites in the synthesis of C9–C24 compounds. Clearly, 8.5CuSi dehydrogenated C6OL to C6K at high rates but in line with its negligible basic properties, almost no new C–C bond was formed. Therefore, the only relevant product was C6H generated by the initial C6OL dehydration since C6K is considered as part of the reactant pool.

On the other hand, the role of the base sites was studied on pure MgO. Results of Table 2 show that the activity for converting the C6O pool was more than hundredfold lower than that of 8.5CuSi, with a significant selectivity to C9–C24 compounds (35.6 %) resulting from coupling reactions.

We have studied the coupling reactions of primary and secondary alcohols and demonstrated that the active site for aldol condensation reactions is a M^{n+}–O^{2-} pair (M = Lewis acid cation) with moderate basic properties. In particular, for Mg–Al mixed oxides with different Mg/Al ratios, a specific combination of acid and base sites, i.e., an adequate balance between Mg^{2+} and Al^{3+} cations generates the best catalytic properties [7, 24, 28]. Thus, Mg-rich Mg–Al oxides with mild basic properties were in general, better catalysts than the strongly basic pure MgO.

In line with these previous studies, the bifunctional metal-base 8.0CuMgAl catalyst was more active and selective to C9–C24 compounds than MgO (Table 2), despite its weaker basicity (Table 1; Fig. 2). This sample,

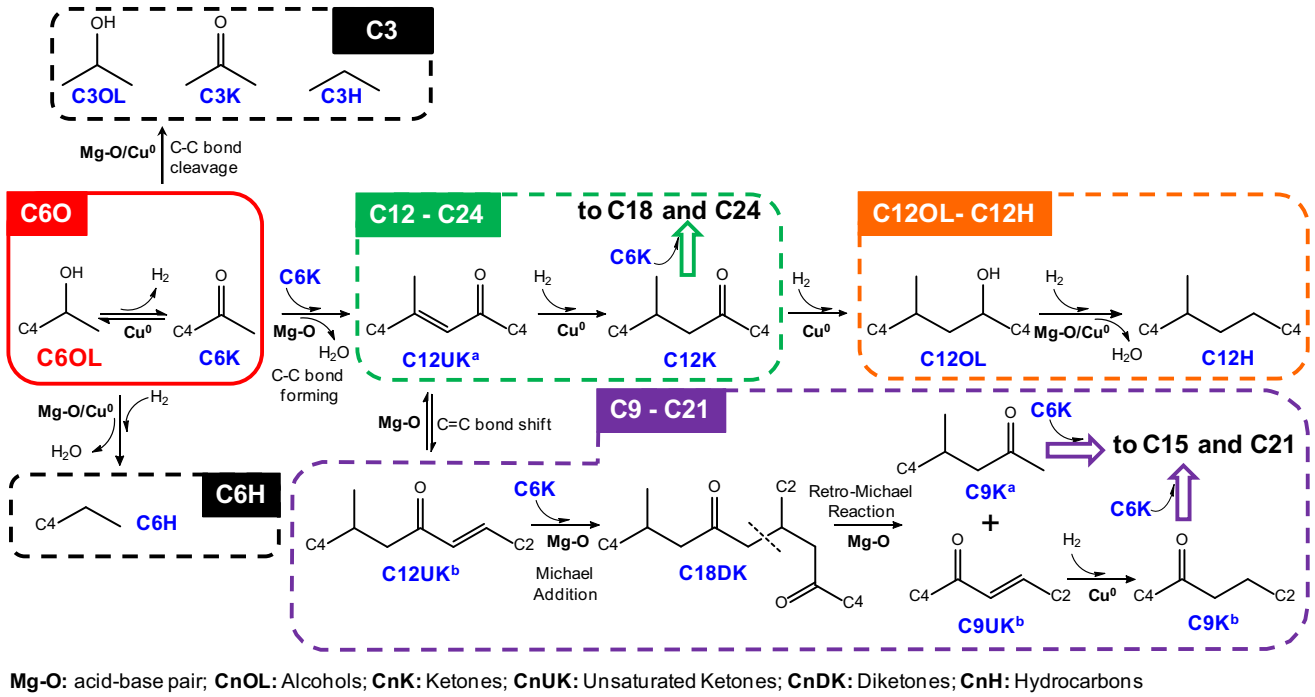

Scheme 1 Reaction steps for the conversion of C6OL on bifunctional 8.0CuMgAl catalyst

Table 2 Activity and selectivity of 8.0CuMgAl, MgO and 8.5CuSi catalysts at 573 K and 101.3 kPa

Catalyst	Catalytic results						
	r_{C6O}[a] (mmol/h g)	TOR[b] (s^{-1}) × 100	S_{C3}[c] (%)	S_{C6H}[c] (%)	S_{C9-C24}[c] (%)	S_{CnO}/S_{CnH}[d] n = 9–24	O/C[e] n = 9–24
8.0CuMgAl	8.42	1.52	3.3	1.7	95.0	8.04	0.067
MgO	0.53	–	0.3	64.1	35.6	1.71	0.053
8.5CuSi	78.46	5.92	0.2	99.5	0.3	0.00	0.000

[a] Reaction rate

[b] Turnover rate per mol surface Cu^0 site

[c] Selectivity at $X_{C6O} \sim 20$ %

[d] Oxygenates/hydrocarbons selectivity ratio for C9–C24 compounds at $X_{C6O} \sim 20$ %

[e] atom ratio in the C9–C24 product pool at $X_{C6O} \sim 20$ %

that contains strong base sites (Mg^{2+}–O^{2-} pairs, Fig. 2) located in a particular chemical environment of the oxide matrix where they are surrounded by Al^{3+} cations, yielded C9–C24 compounds with 95 % selectivity and almost completely suppressed formation of C6H. Although lower than on 8.5CuSi, the r_{C6O} and TOR values on sample 8.0CuMgAl reveal the participation of the Cu^0 particles in the formation of heavy compounds. Surface Cu^0 species promote the preferential hydrogenation of C6OL to C6K by activating the alcohol O–H bond at higher rates than the C–O or C–C bonds that would have given rise to dehydration or short chain undesirable products, respectively. Thus, the surface coverage of C6K species that initiate the aldol condensation sequence (block C6O, Scheme 1) is expected to be substantially higher on the bifunctional 8.0CuMgAl catalyst than on pure MgO, thereby explaining the higher selectivity to C9–C4 aldol condensation products. Scheme 1 summarizes the role played in the reaction sequence by both surface active species: the metallic Cu^0 particles and the Lewis acid cation-oxygen anion pair site.

As a consequence of the higher surface coverage of oxygenates formed by C–C coupling reactions (mainly C12O), Table 2 shows that the oxygenates/hydrocarbons (S_{CnO}/S_{CnH}) selectivity ratio for C9–C24 compounds is higher on the bifunctional metal-base 8.0CuMgAl catalyst compared to MgO.

Table 2 shows that the calculated O/C atom ratio in the C9–C24 product pool obtained on catalyst 8.0CuMgAl was 0.067, a much smaller value than that of C6OL (0.167). This result confirms that the strategy chosen here to upgrade biomass resources notoriously decreases the O/C ratio of 0.8 in cellulose or 1.0 in monosaccharide sugars, and gives a product mixture with superior hydrophobic properties than C6OL [29].

3.3 Product Distribution

Product formation on the bifunctional catalyst 8.0CuMgAl was further studied at different contact times (W/F^0_{C6OL}, g cat. h mol^{-1}) in order to elucidate the reaction pathways leading to C9–C24 compounds. Figure 4a shows the evolution of the C6O reactant pool conversion (X_{C6O}, %) and yields (Y, %) toward C9–C24, C3 and C6H products as a function of W/F^0_{C6OL} at typical reaction conditions, i.e., 573 K, 101.3 kPa and N_2:C6OL = 97.2:4.1 = 23.7 (molar). Almost total conversion (92 %) was achieved at W/F^0_{C6OL} = 500 g h mol^{-1} whereas the highest $Y_{C9–C24}$ was 79 % at 350 g h mol^{-1}; $Y_{C9–C24}$ decreased at higher contact times as the result of the increasing formation of C3 and C6H compounds.

The product distribution for these reactions carried out in N_2 is presented in Fig. 5 as the yields of C9–C24 products organized as even and odd carbon atom number products. C12 and C9 compounds were the main products reaching 55 % of the total products at the highest conversions. Apart from C12 and C9 compounds, C15 and C18 compounds were quantified, as well as minor amounts of C21 and C24 products.

The shape of the C12 yield curve showing a non-zero initial slope (at $W/F^0_{C6OL} \rightarrow 0$) suggests direct C12 formation from C6K via the first aldol condensation sequence depicted in Scheme 1, leading to formation of C12UK[a], C12K, C12OL and C12H compounds. At higher W/F^0_{C6OL} values the slope of the C12 yield curve decreased as C12 compounds transform into heavier compounds by consecutive aldol condensations, Scheme 1. The lower initial slope of the C18 and C24 yield curves respect to that of C12 confirms that they are secondary products formed from C12.

The results obtained at different W/F^0_{C6OL} on the bifunctional 8.0CuMgAl catalyst are consistent with the reaction network depicted in Scheme 1 for the upgrading of 2-hexanol to C9–C24 compounds. Initially, C6OL is dehydrogenated on Cu^0 sites forming the saturated ketone

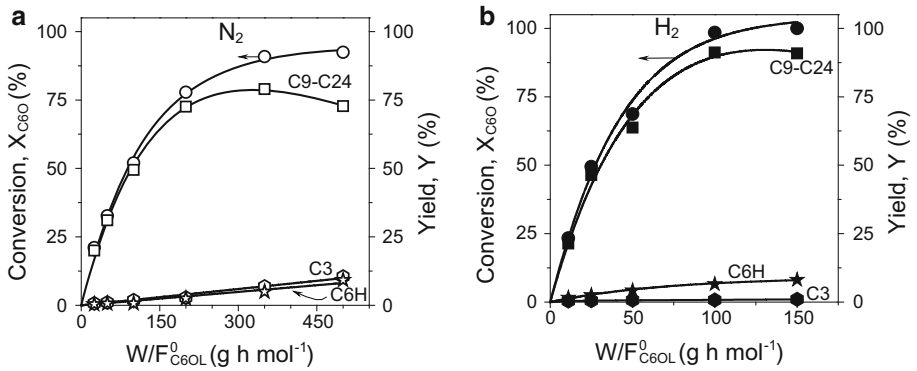

Fig. 4 Effect of contact time (W/F^0_{C6OL}) on conversion and yields to C9–C24, C6H and C3 products for the reactions carried out in **a** N_2 and **b** H_2 (catalyst: 8.0CuMgAl, T = 573 K, P = 101.3 kPa, $\bar{P}_{C6OL}$ = 4.1 kPa)

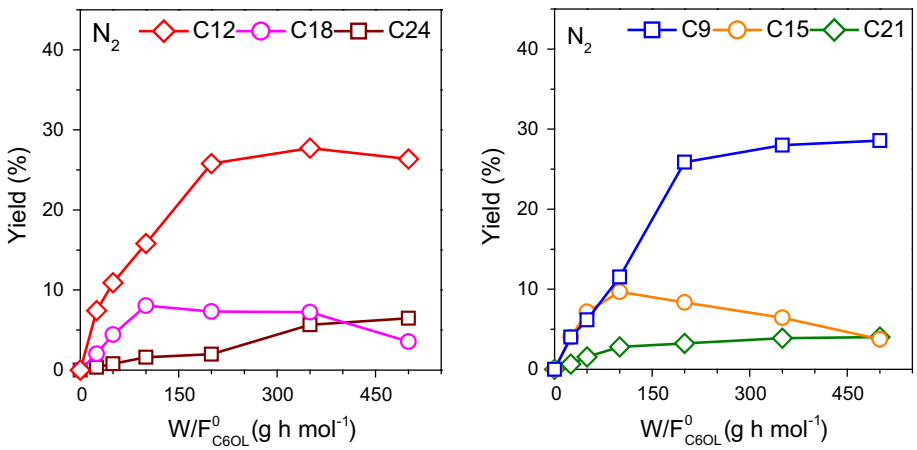

Fig. 5 Effect of contact time (W/F^0_{C6OL}) on the yields toward Cn products (n = 9, 12, 15, 18, 21 and 24) (catalyst: 8.0CuMgAl, T = 573 K, P = 101.3 kPa, N_2/C6OL = 23.7)

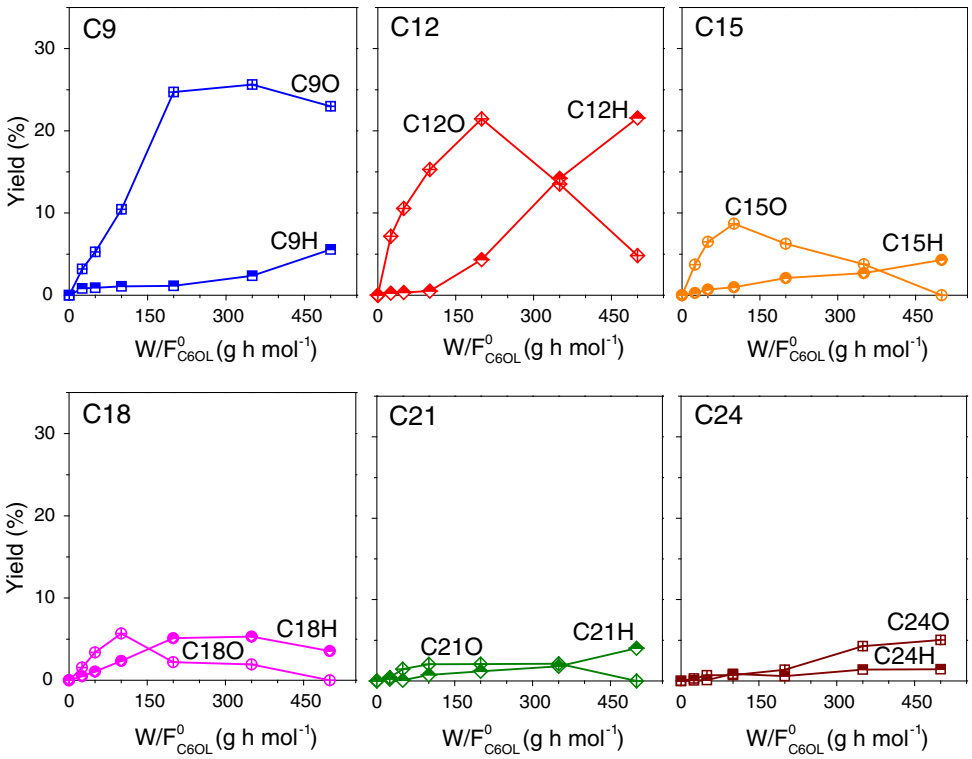

Fig. 6 Effect of contact time (W/F^0_{C6OL}) on the yields toward oxygenates (CnO) and hydrocarbons (CnH) (n = 9, 12, 15, 18, 21 and 24) (catalyst: 8.0CuMgAl, T = 573 K, P = 101.3 kPa, N_2/C6OL = 23.7)

C6 K. Then, the C–C bond forming aldol condensation of C6K on Mg^{2+}–O^{2-} pairs forms an aldol adduct (a hydroxyketone not shown) that is readily dehydrated to the α,β-unsaturated ketone C12UK[a]; the latter can be hydrogenated to saturated C12K. Consecutive hydrogenation and dehydration steps convert C12K in an alcohol (C12OL) and a hydrocarbon (C12H). A second and a third aldol condensation sequence can take place by reaction of C12K with another C6K molecule to give ketones, alcohols and hydrocarbons with an even number of carbon atoms, such as C18 and C24.

Formation of products with an odd number of carbon atoms such as C9, C15 and C21 cannot be explained by the reaction sequence described above and therefore, a different reaction pathway needs to be postulated. One possibility is the coupling of C3 oxygenates with C6K to give C9 compounds. However, results of Fig. 4a show that the yield of C3 compounds formed by C–C bond cleavage reactions is not enough (<10 %) to give the high yields of C9 products shown in Fig. 5. In addition, the shape of the Y_{C3} curve showing no slope change, confirms that C3 compounds are hardly converted in other products. Kunkes et al. [21] found odd carbon atom number compounds during conversion of hexanone on a Pd/$CeZrO_x$ catalyst and postulated an alternative pathway, depicted as the C9–C21 block of Scheme 1. This pathway starts by isomerization of the α,β-unsaturated ketone C12UK[a] giving C12UK[b]. Although unsaturated ketones were not detected among the reaction products, it has to be remarked that in previous works we reported that α,β-unsaturated ketones are unstable reaction intermediates that rapidly convert into other products on similar bifunctional metal-base catalysts. We have shown [9, 30, 31] that in the absence of molecular hydrogen in the feed, the base-catalyzed C=C bond shift is a fast reaction that competes with the Cu^0-promoted C=C bond reduction toward C12K, thereby supporting formation of C12UK[b]. Consecutive base-catalyzed Michael and retro-Michael reactions convert C12UK[b] in C9K, after which conventional aldol condensation steps lead to C15 and C21 products. The shape of the C15 and C21 yield curves in Fig. 5 confirms their formation from C9.

In Fig. 6 the yields of C9–C24 products for the reactions carried out in N_2 are presented as a function of the contact time and discriminated between oxygenates and hydrocarbons. From the slope of the curves at $W/F^0_{C6OL} \rightarrow 0$ it can be inferred that hydrocarbons are secondary products clearly formed from oxygenates, in agreement with the pathways of Scheme 1. In fact, calculations of the formation rates for the C9–C24 products at initial conditions ($W/F^0_{C6OL} \rightarrow 0$), Table 3, show a much higher value for oxygenates ($r^0_{CnO} = 8.1$ mmol g^{-1} h^{-1}) compared with hydrocarbons ($r^0_{CnH} = 0.9$ mmol g^{-1} h^{-1}) therefore confirming that oxygenates are primary products.

Main products at high conversions were C12H and C9O. The lack of significant amounts of alkanes other than C12H

Table 3 Effect of co-feeding H_2 on the initial reaction rates (r^0), product distribution and oxygen content

Reaction atmosphere	r^0_{C6O} (mmol/hg)	C9–C24 products					
		r^0_{C9-C24} (mmol/hg)	r^0_{CnO} (mmol/hg)	r^0_{CnH} (mmol/hg)	O/C[a]	O/C[b]	S_{CnO}/S_{CnH}[c]
N_2	9.6	9.0	8.1	0.9	0.067	0.035	0.82
H_2	25.8	23.7	21.2	2.5	0.071	0.010	0.17

Catalyst: 8.0CuMgAl, T = 573 K, $N_2(H_2)$/C6OL = 23.7 (molar), n = 9-24

[a] Atom ratio at $X_{C6O} \sim 20$ %

[b] Atom ratio at $X_{C6O} \sim 100$ %

[c] Oxygenates/hydrocarbons selectivity ratio at $X_{C6O} \sim 100$ %

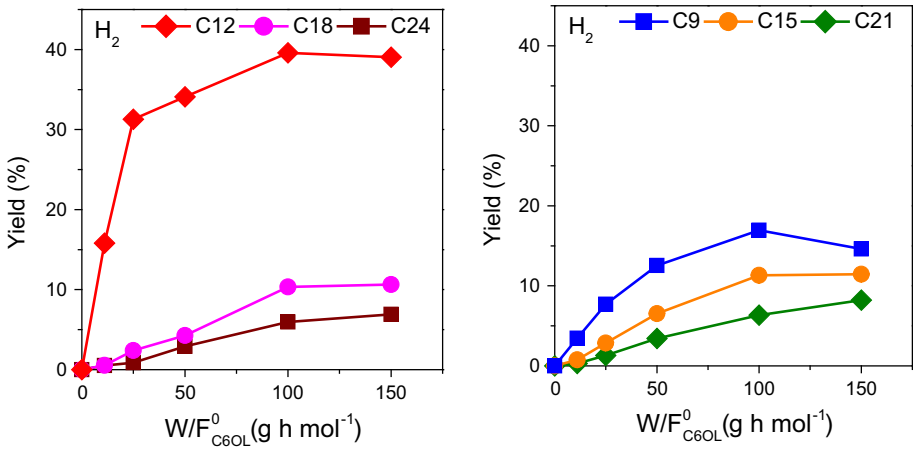

Fig. 7 Effect of contact time (W/F^0_{C6OL}) on the yields toward Cn products (n = 9, 12, 15, 18, 21 and 24) (catalyst: 8.0CuMgAl, T = 573 K, P = 101.3 kPa, H_2/C6OL = 23.7)

is explained by the deficient amount of surface hydrogen species available to reduce the C=O bond of ketones formed after C12 compounds (C9, C15, C18, C21 and C24 ketones). This occurs because under these reactions conditions the only source of hydrogen is the initial C6OL dehydrogenation to C6K.

3.4 Effect of Co-feeding H_2 on the Reaction Pathways and on the Catalyst Activity and Product Distribution

The purpose of the present work is to upgrade 2-hexanol by converting it in high molecular weight compounds with low oxygen content. However, the results of Fig. 6 indicated some limitations for oxygen removal when only surface-generated hydrogen species are available for hydrogenation of oxygenates. Thus, we carried out additional experiments with sample 8.0CuMgAl at different W/F^0_{C6OL} to investigate the effect of co-feeding H_2 to the reactor in a H_2/C6OL molar ratio of 23.7, similar to the one used in the experiments under inert atmosphere.

Figure 4b shows that clearly, the catalyst activity was much higher in H_2 than in N_2 since total conversion was reached in H_2 at $\sim$100 g h mol^{-1}. The yield to C9–C24 products was also higher in H_2 than in N_2; the highest Y_{C9-C24} in H_2 was 91 % in contrast to 79 % in N_2. The enhanced Y_{C9-C24} in H_2 is the consequence of the negligible formation of C_3 compounds ($Y_{C3} < 1$ %) what suggests that undesirable C–C bond breaking reactions are not favored. On the other hand, the dehydration-hydrogenation pathway that leads to C6H was not significantly affected by the presence of molecular H_2 in the feed. These high Y_{C9-C24} values obtained in H_2 at atmospheric pressure conditions compare favorably with the 66 % yield to C9–C18 products reported by Kunkes et al. [21] for the conversion of C6K in H_2 on a 0.25 wt% $PdCeZrO_x$ catalyst at 623 K and 5 bar, or with the 86 % yield to C12–C18 products reported by West et al. [32] for the conversion of the same feed at 573 K and 5 bar on a Cu–Mg–Al mixed oxide.

From the slopes of the curves of Fig. 4 at $W/F^0_{C6OL} \rightarrow 0$, the initial overall reaction rate (r^0_{C6O}, mmol h^{-1} g^{-1}) as well as the initial rate of C9–C24 product formation (r^0_{C9-C24}, mmol h^{-1} g^{-1}) were calculated for both, the reactions carried out in N_2 and in H_2. Table 3 summarizes the results. The much higher values of r^0_{C6O} and r^0_{C9-C24} measured in H_2 suggest participation of hydrogen in the rate-limiting step of C9–C24 product formation and a positive hydrogen reaction order in the kinetic rate expression.

Figure 7 presents the yields of C9–C24 products grouped as even and odd carbon atom number products for

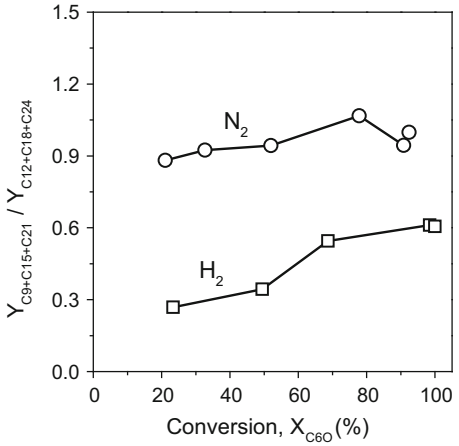

Fig. 8 Odd/even carbon atom number compound ratio as a function of conversion for the reactions carried out in N_2 and H_2 [catalyst: 8.0CuMgAl, T = 573 K, P = 101.3 kPa, $N_2(H_2)$/C6OL = 23.7]

the catalytic tests in H_2. C12 compounds were the main products regardless of the conversion level in contrast to the results of Fig. 5 showing similar amounts of C12 and C9 products in N_2. Furthermore, Fig. 8 shows that odd carbon atom number products (C9, C15 and C21) were obtained in lower yields for the reactions carried out in H_2 when compared, at similar conversion levels, with the reactions in N_2. As a consequence, at conversions near 100 % the average molecular weight of the C9–C24 product fraction was higher in H_2 than in N_2.

All these results suggest that different reaction networks apply in N_2 or in H_2, with the first step of the pathway toward C9K formation (Scheme 1) being the main difference. In the presence of molecular H_2 in the feed, the C=C bond of C12UK[a] is rapidly reduced on Cu^0 sites forming the saturated ketone C12K, enabling then the route to other even carbon atom number compounds (Scheme 1, blocks C12–C24 and C12OL–C12H) and hampering the alternative route toward C9K formation via the C=C bond shift of C12UK[a]. In contrast, when the reaction is carried out in N_2 the catalyst surface contains only surface-generated hydrogen formed by the initial C6OL dehydrogenation to C6K, thereby facilitating the competing C=C bond migration route toward odd carbon atom number products (Scheme 1, block C9–C21).

The distribution of C9–C24 oxygenates and hydrocarbons for the reactions carried out in H_2 is plotted as a function of the contact time in Fig. 9. Although in Table 3 the calculations of the initial oxygenate (r^0_{CnO}) and hydrocarbon (r^0_{CnH}) formation rates reveal that they are 3 times higher than in N_2, the presence of hydrogen does not change the contribution of alkanes to the product pool under initial conditions since the r^0_{CnH}/r^0_{C6OL} ratio was comparable in both reaction atmospheres. Correspondingly, the values of the O/C ratio in the C9–C24 product pool at $X_{C6O} \sim 20$ % were similar. The effect of H_2 is more evident as W/F^0_{C6OL} increases due to the enhanced formation of hydrocarbons by hydrogenation of

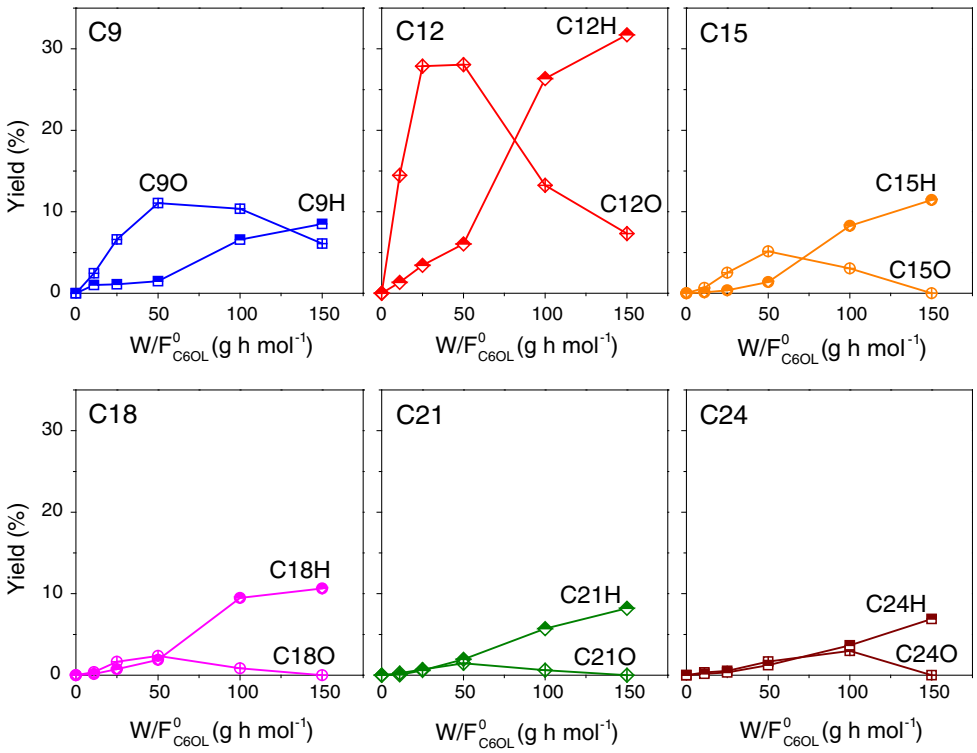

Fig. 9 Effect of contact time (W/F^0_{C6OL}) on the yields toward oxygenates (CnO) and hydrocarbons (CnH) (n = 9, 12, 15, 18, 21 and 24) (catalyst: 8.0CuMgAl, T = 573 K, P = 101.3 kPa, H_2/C6OL = 23.7)

oxygenates, Fig. 9. For instance, the S_{CnO}/S_{CnH} oxygenates/hydrocarbons selectivity ratio for C9–C24 products at $X_{C6O} \sim 100$ % decreased from 0.82 in N_2 to 0.17 in H_2, Table 3. C12H was the main product at 100 % conversion but heavier alkanes were also formed in significant amounts in contrast to the results obtained in N_2. Thus, the oxygen content of the C9–C24 product pool calculated as the O/C ratio was 0.010 at $X_{C6O} \sim 100$ %, a value substantially lower than the one under inert atmosphere (0.035), Table 3.

4 Conclusions

A Cu–Mg–Al mixed oxide (8.0CuMgAl) with moderate basic properties and 8 wt% Cu promote the gas-phase upgrading of 2-hexanol to heavier compounds at high rates. Products are a hydrophobic mixture of C9–C24 oxygenates and hydrocarbons with applications as liquid transportation fuels. In the mixture composed of branched alcohols, ketones and alkanes, the O/C atom ratio is as low as 0.01.

Formation of C9–C24 compounds occurs by bifunctional metal-base catalysis through a complex reaction network that involves tandem dehydrogenation, C–C bond formation, dehydration and hydrogenation reactions. Cu^0 particles promote dehydrogenation and hydrogenation steps whereas Mg–O pairs surrounded by Al cations participate mainly in the C–C coupling by aldol condensation.

Pure MgO, containing strong base sites, forms C9–C24 products at low rates whereas an 8.5 wt% Cu/SiO_2 catalyst, presenting just metallic copper particles, is much more active but only dehydrogenates C6OL to C6K without promoting the C–C bond formation. On the bifunctional 8.0CuMgAl catalyst, C9–C24 yields of up to 91 % are obtained under mild reaction conditions (573 K, 101.3 kPa, H_2 atmosphere).

The 2-hexanol upgrading can be performed under inert (N_2) or reducing (H_2) reaction atmospheres but reaction rates are much higher in H_2; the use of N_2 enables a reaction pathway leading to odd carbon atom number compounds and therefore decreases the average molecular weight of the C9–C24 product pool. The use of H_2, on the other hand, increases the contribution of hydrocarbons in the C9–C24 fraction.

Acknowledgments Authors thank Agencia Nacional de Promoción Científica y Tecnológica (ANPCyT), Argentina (Grant PICT 1888/10), CONICET, Argentina (Grant PIP 11220090100203/10) and Universidad Nacional del Litoral, Santa Fe, Argentina (Grant CAID PI 64-103/11) for financial support of this work.

References

1. Corma A, Iborra S, Velty A (2007) A Chem Rev 107:2411–2502
2. Bond JQ, Alonso DM, Dumesic JA (2013) In: Wyman CE (ed) Aqueous pretreatment of plant biomass for biological and chemical conversion to fuels and chemicals, 1st edn. Wiley, New York
3. Chheda JN, Dumesic JA (2007) Catal Today 123:59–70
4. Serrano-Ruiz JC, Dumesic JA (2011) Energy Environ Sci 4:83–99
5. Simonetti DA, Dumesic JA (2008) ChemSusChem 1:725–733
6. Kunkes EL, Simonetti DA, West RM, Serrano-Ruiz JC, Gärtner CA, Dumesic JA (2008) Science 322:417–421
7. Di Cosimo JI, Torres G, Apesteguía CR (2002) J Catal 208:114–123
8. Torres G, Apesteguía CR, Di Cosimo JI (2007) Appl Catal A 317:161–170
9. Di Cosimo JI, Acosta A, Apesteguía CR (2004) J Mol Catal A 222:87–96
10. Torresi PA, Díez VK, Luggren PJ, Di Cosimo JI (2014) Catal Sci Technol 4:3203–3213
11. Bravo-Suarez JJ, Subramaniam B, Chaudhari RV (2013) Appl Catal A 455:234–246
12. Marcu IC, Tichit D, Fajula F, Tanchoux N (2009) Catal Today 147:231–238
13. Zhou M, Zeng Z, Zhu H, Xiao G, Xiao R (2014) J Energy Chem 23:91–96
14. Tanasoi S, Tanchoux N, Urda A, Tichit D, Sandulescu I, Fajula F, Marcu IC (2009) Appl Catal A 363:135–142
15. Chmielarz L, Jabłonska M, Struminski A, Piwowarska Z, Wegrzyn A, Witkowski S, Michalik M (2013) Appl Catal B 130–131:152–162
16. Chmielarz L, Piwowarska Z, Rutkowska M, Wojciechowska M, Dudek B, Witkowski S, Michalik M (2012) Catal Commun 17:118–125
17. Di Cosimo JI, Díez VK, Apesteguía CR (1996) Appl Catal A 13:149–166
18. Torresi PA, Díez VK, Luggren PJ, Di Cosimo JI (2013) Appl Catal A 458:119–129
19. Monti DA, Baiker A (1983) J Catal 83:323–335
20. Malet P, Caballero A (1988) J Chem Soc Faraday Trans I 84:2369–2375
21. Kunkes EL, Gürbüz EI, Dumesic JA (2009) J Catal 266:236–249
22. Díez VK, Torresi PA, Luggren PJ, Ferretti CA, Di Cosimo JI (2013) Catal Today 213:18–24
23. Luggren P (2015) PhD Thesis, Universidad Nacional del Litoral
24. Di Cosimo JI, Díez VK, Xu M, Iglesia E, Apesteguía CR (1998) J Catal 178:499–510
25. Díez VK, Apesteguía CR, Di Cosimo JI (2003) J Catal 215:220–233
26. Di Cosimo JI, Apesteguía CR (1994) J Mol Catal 91:369–386
27. Boccuzzi F, Chiorino A, Martra G, Gargano M, Ravasio N, Carrozzini B (1997) J Catal 165:129–139
28. Di Cosimo JI, Apesteguía CR, Ginés MJL, Iglesia E (2000) J Catal 190:261–275
29. Choudhary TV, Phillips CB (2011) Appl Catal A 397:1–12
30. Di Cosimo JI, Acosta A, Apesteguía CR (2005) J Mol Catal A 234:111–120
31. Braun F, Di Cosimo JI (2006) Catal Today 116:206–215
32. West RM, Kunkes EL, Simonetti DA, Dumesic JA (2009) Catal Today 147:115–125